Journal of Materials Chemistry A

ROYAL SOCIETY OF CHEMISTRY

PAPER

View Article Online
View Journal | View Issue

Cite this: J. Mater. Chem. A, 2026, 14, 21234

Concentration dependent salt-polymer-dynamic bond interactions dictate non-monotonic conductivity and viscoelasticity in vitrimer electrolytes

Samyak N. Chordia,[ab] Paul V. Braun,[ab] Shailesh N. Joshi,[bc] Timothy S. Arthur,[d] Yu-Hsuan Tsao[ab] and Christopher M. Evans *[ab]

Vitrimer electrolytes (VEs) are an emerging class of solid polymer electrolytes that couple dynamic covalent bond exchange with high ionic conductivity to mitigate lithium dendrite formation while enabling self-healing and recyclability. Here, VEs with ethylene oxide (EO) chains and dynamic imine crosslinks were synthesized to systematically determine how crosslink density and LiTFSI salt concentration dictate viscoelasticity and ionic conductivity. The VEs exhibit a non-monotonic dependence of relaxation times and ionic conductivity on crosslink density at fixed salt. Variations in salt concentration at fixed crosslink density resulted in doubly non-monotonic trends with three distinct regimes in modulus and relaxation times which increase, decrease, and then increase again with added salt (r = 0.1 to 0.5). Ionic conductivity showed the inverse of these trends, attributed to the complex interplay between segmental dynamics, catalyzed bond exchange and ion aggregation. Wide-angle X-ray scattering revealed ionic aggregate peaks which support the picture of fewer free Li ions leading to lower conductivity, longer relaxation times, and higher modulus. In contrast, the glass transition temperature (T_g) continuously increased with salt. All VEs were amorphous with a plateau modulus above 10^5 Pa and ionic conductivities exceeding that of linear PEO by an order of magnitude. This work establishes key design principles linking dynamic bond exchange and salt content to the viscoelasticity and conductivity for next-generation vitrimer electrolytes.

Received 12th January 2026
Accepted 13th April 2026

DOI: 10.1039/d6ta00316h

rsc.li/materials-a

Introduction

The global market for lithium-ion batteries has been increasing rapidly since the last decade and is expected to provide about 9300 GWh of energy by 2030.[1] Lithium metal offers a high theoretical specific capacity of 3860 mAh g^{-1} and low density of 0.59 g cm^{-3}, making it a promising candidate for high energy-density storage applications[2–6] including consumer electronics, portable devices and electric vehicles.[7,8] However, during battery cycling the heterogeneous deposition of lithium ions at the anode – electrolyte interface promotes nucleation, leading to the growth of tree-like metallic lithium dendrites which propagate, penetrating through the electrolyte, and cause a short-circuit with catastrophic failure of the battery.[6,9–13] Solid-state electrolytes are emerging as leading contenders for next-generation battery technologies, as they are less flammable and susceptible to leakage,[5,14–17] while also exhibiting mechanical properties capable of suppressing dendrite growth and extending the operational lifetimes.[18–20] Poly(ethylene oxide) (PEO) based polymer electrolytes have been extensively studied due to their Li^+ solvation capability, where the ether oxygens in the EO chains undergo coordination with the positive charged Li^+ cation, promote salt dissociation and enable ion transport.[21–24] However, linear PEO is semi-crystalline at room temperature with low ionic conductivity (typically 10^{-7}–10^{-5} S cm^{-1}) and the modulus decreases sharply in the molten state allowing dendrite propagation.[25–27] To overcome the above limitations, permanently crosslinked PEO networks have been studied and can show higher ionic conductivity, little or no crystallinity, and higher modulus (>10^5 Pa) leading to longer-term cycling before failure.[18,28–35] Recent work has incorporated dynamic covalent bonds as crosslinks in network electrolytes, with the goal of enabling reprocessability, reuse of the material after failure.[36–42]

Dynamic covalent chemistries including boronic esters,[43–46] vinylogous urethanes,[47–50] and imines[51–56] undergo an associative exchange mechanism, such that the bond does not first break before exchanging polymer chains. Such networks are

[a]Department of Materials Science and Engineering, University of Illinois Urbana Champaign, Urbana, Illinois 61801, USA. E-mail: cme365@illinois.edu
[b]Materials Research Laboratory, University of Illinois Urbana Champaign, Urbana, Illinois 61801, USA
[c]Electronics Research Department, Toyota Research Institute of North America, Ann Arbor, Michigan 48105, USA
[d]Materials Research Department, Toyota Research Institute of North America, Ann Arbor, Michigan 48105, USA

often called vitrimers and have received increased recent attention as solid polymer electrolytes capable of prolonged cell cycling.[57–61] Bond exchange is also expected to mitigate the large stresses and volume changes that occur during cycling. As the material flows and reconfigures, typically at elevated temperatures, the electrolyte can adapt to pressure and changes in the electrode surface to retain interfacial stability. Recent studies on vitrimer electrolytes (VEs), have primarily focused on evaluating properties such as self-healing in response to a cut or damage,[62–65] mechanical robustness[66] and ionic conductivity.[61,67] However, the effect of crosslinking density and varying salt concentration on the viscoelasticity and ionic conductivity has not been systematically investigated. Balsara *et al.* investigated ionic conductivity over a broad range of salt concentrations ($r = Li^+/EO$ from 0.01 to 0.5) in PEO homopolymers and block copolymer electrolytes and observed a non-monotonic trend with r due to competing effects of added ions and increased T_g.[68–71] In VEs, additional contributions arise as salt catalyzes bond exchange and can coordinate with dynamic bonds, leading to different trends of conductivity with r, as well as the bulk viscoelasticity of the network.

In this work, a series of PEO vitrimer electrolytes with dynamic imine crosslinks were synthesized with varying crosslinking density (M_n = 1000, 2000 and 6000 g mol^{-1} of PEO) and salt concentrations (r = 0.1 to 0.5) to probe their impact on the bulk relaxation, glass transition temperature (T_g), rubbery modulus, and ionic conductivity. Shear rheological experiments revealed that bulk relaxation times (crossover of storage and loss modulus prior to flow, $\tau_{crossover}$) decrease with increasing crosslinking density for neutral vitrimer networks, due to an increase in T_g and reduced segmental mobility. At a fixed r = 0.1, a non-monotonic trend emerges in relaxation times and ionic conductivity even when normalized by T_g. Next, the concentration of LiTFSI was systematically varied up to $r = 0.5$ with fixed 2000 g mol^{-1} PEO to determine the impacts on modulus, bulk relaxation and conductivity. The rubbery plateau modulus (G') remained above 10^5 Pa for salt concentrations up to $r = 0.3$, large enough to contribute to dendrite suppression. Ionic conductivity as a function of r displayed a maximum at 0.1, consistent with observations in PEO/LiTFSI system,[68,71] while $\tau_{crossover}$ was fastest at $r = 0.1$. Ionic conductivity showed three distinct regimes where values first decreased from r = 0.1–0.125, increased from r = 0.125–0.15, and then decreased going to $r = 0.5$. These same regimes were observed for $\tau_{crossover}$ and G' but with opposite direction as values increase, decrease, then increase at the same r values as for conductivity. The T_g monotonically increased with r and lead to low conductivity/longer $\tau_{crossover}$ in the r = 0.3–0.5 region. Conductivity, modulus, and relaxation times were measured between 30–130 °C to span regimes relevant to applications as well as higher temperatures where bond exchange is significantly accelerated. At lower salt concentrations, WAXS reveals a non-monotonic behavior of the ionic aggregate peak relative to the amorphous halo, as salt can interact with the EO backbone, dynamic imine bond, or aggregate. Higher intensity aggregation peaks correspond to low conductivity and slow $\tau_{crossover}$ as fewer free Li ions are able to conduct or catalyze imine exchange. ^{7}Li NMR experiments were also conducted to probe the local environment of lithium and indicate Li-imine coordination is most prevalent for $r = 0.1$. At higher r, the peaks are largely invariant and similar to those for pure LiTFSI salt.

Experimental section

Materials

Poly(ethylene glycol) diamine (NH_2-PEG-NH_2) was purchased from Biopharma PEG (M_n = 1000 g mol^{-1}, > 95%) or Sigma-Aldrich (M_n = 2,000, 6000 g mol^{-1}). Benzene-1,3,5-tricarbaldehyde (BTA, 97%) was purchased from Combi-Blocks, Inc. Poly(ethylene oxide) (PEO, M_v = 100 000 g mol^{-1}), lithium bis(trifluoromethanesulfonyl)imide (LiTFSI, 99.99% trace metals basis) and anhydrous acetonitrile (ACN, 99.8%) were purchased from Sigma-Aldrich. All chemicals were used as received without further purification.

Synthesis of imine dynamic networks

Telechelic polymer networks crosslinked with dynamic imine bonds were synthesized using poly(ethylene glycol) diamine and benzene-1,3,5-tricarbaldehyde (BTA) *via* the Schiff-base reaction. Diamine (0.1 mmol) was weighed in a 4 mL glass vial and then dissolved in anhydrous ACN (0.8 mL). The solution was placed on a vortex mixer for 30 s until transparent. Subsequently, BTA (0.067 mmol) and LiTFSI salt $\left(\text{with a ratio } r = \frac{[Li^+]}{[EO]} = 0.1 - 0.5\right)$ was added to the solution and was sonicated for 2 h to ensure homogenous mixing. Stoichiometry of the amine:aldehyde groups was fixed at 1 : 1 to promote high conversion of functional groups. After mixing, the solution was quickly transferred into a PTFE mold and dried at room temperature for 4 h until a film was obtained. Finally, samples were dried at 60 °C for 24 h in air followed by drying at 80 °C for another 24 h under vacuum to remove excess acetonitrile and water. The vitrimer electrolytes were named VE-x, where x indicates the average molecular weight of PEO between crosslinks. The ratio between lithium salt and ethylene oxide repeat units was first fixed at $r = 0.1$ to understand the effect of crosslinking density on viscoelasticity and ionic conductivity. Next, the molecular weight of PEO was fixed at 2000 g mol^{-1} and salt concentration was varied from r = 0.1 to 0.5 and were named as VE-2k-r. Neutral vitrimer networks were synthesized by the same procedure without adding salt and were named V-x. All samples were stored in a glovebox after drying for further use.

Synthesis of linear PEO/LiTFSI electrolyte

The PEO powder was dried initially at 45 °C in a vacuum oven for 24 h and LiTFSI salt was dried at 100 °C in a vacuum oven for 24 h to remove moisture. Post drying, the PEO powder (0.5 g) and LiTFSI salt (0.326 g) was ground using a mortar and pestle until a uniform mixture was achieved. The mixture was heated in a glass vial at 80 °C on a hot plate and stirred with a spatula until a soft paste was obtained, followed by overnight drying at 80 °C in a vacuum oven. The salt concentration was fixed at r =

0.1. The electrolyte was formed by pressing the viscous paste between two Teflon (PTFE) sheets with a spacer on a hot plate at 80 °C inside a glove box and stored inside for further use.

Attenuated total reflection-fourier transform infrared spectroscopy (ATR-FTIR)

Infrared spectra were obtained using a Bruker ALPHA FT-IR spectrometer equipped with a platinum-ATR QuickSnap sampling module. All measurements were carried out at room temperature. The spectra were collected over the range of 4000–400 cm^{-1}, with each spectrum recorded over 32 scans at a resolution of 4 cm^{-1}.

^{7}Li solid-state NMR

^{7}Li NMR spectra were obtained using a Bruker NEO spectrometer operating at magnetic field of $B_0 = 11.7$ T ($\nu_L(^7Li) = 194.25$ MHz). A 6 mm Phoenix HXY magic-angle spinning (MAS) probe was used for all measurements at a spinning speed of 5 kHz at room temperature. Samples were packed into Kel-F inserts and subsequently placed into a 6 mm outer diameter zirconia rotors. The selective ^{7}Li p/2 pulse width was set to 4.8 μs, with a recycle delay of 2 s. Each spectrum was acquired with 64 transients. The ^{7}Li NMR chemical shifts were referenced to 1 M LiCl in D_2O (d = 0 ppm). mNOVA software was used to determine chemical shifts and assign peaks of the collected spectra. For Li-Im, r is defined as the ratio of [Li^+] to [small imine molecule].

Wide-angle X-ray scattering (WAXS)

Bulk samples of vitrimer electrolytes were measured using a custom-built Wide-angle X-ray scattering machine (Forvis Technologies, CA, USA) composed of a Xenocs Genix3D Cu-Ka X-ray source (50 kV, 0.6 mA) with a divergence of ~1.3 mrad. This 2D diffraction data were collected by an Eiger 2R_500K detector (pixel size 75 μm × 75 μm), radially averaged, and integrated using FIT2D software. The distance between the sample and detector was approximately 140 mm and calibrated with silver behenate before measurement. Each sample was measured for 600 s at room temperature, except the neutral networks which were heated to 70 °C (above T_m) to remove the effect of PEO crystal scattering.

Differential scanning calorimetry (DSC)

Differential scanning calorimetry (DSC Q2500, TA Instruments) samples weighing 5–7 mg were prepared and hermetically sealed in Tzero pans in a glovebox to minimize moisture effects. The samples were then subjected to a heat–cool–heat cycle over a temperature range of −100 °C to 100 °C at a rate of 10 °C min^{-1}. The T_g values were determined from the midpoint of the change in heat capacity (1/2 ΔC_p) criterion from the second heating cycle.

Thermogravimetric analysis (TGA)

Thermal stability was determined by TGA (Q50, TA Instruments) heating from 30 °C to 600 °C at 10 °C min^{-1} under N_2. The degradation temperature (T_d) was determined at 5% mass loss.

Electrochemical impedance spectroscopy

Electrochemical impedance spectroscopy (EIS) was performed using a Bio-Logic SP300 potentiostat equipped with a Controlled Environment Sample Holder and Intermediate Temperature System. Spectra were collected by applying a 20 mV amplitude with a frequency range of 1 MHz to 100 mHz. The real conductivity (σ') was calculated from the complex impedance, $Z^*(w) = Z' + i\omega Z''$, using the following equation:

$$\sigma'(w) = \frac{l}{A} \times \frac{Z'(w)}{\left[Z'(w)^2 + Z''(w)^2\right]}$$

Here, l is the film thickness, A is the area, and ω is the frequency. All samples were prepared using CR2032 coin cells, assembled according to a protocol outlined in prior literature.[45] Temperature-dependent impedance measurements were conducted from 130 °C to 30 °C in 10 °C increments, after equilibrating at the highest temperature.

Oscillatory shear rheology

Prior to each rheological measurement, the samples were prepared as 8 mm diameter discs with thickness ranging from 700 to 900 μm using a stainless-steel mold at 120 °C on a hot plate and applying a 5 kg load for 2 h inside a glovebox. The specimens were then loaded onto a stress-controlled TA Instruments DHR-2 rheometer with a parallel plate geometry, preheated to 130 °C. Frequency sweep experiments were carried out on each network from 100 to 0.01 rad s^{-1} at 10 °C intervals from 130 °C to 30 °C with an applied strain of 1%. Temperature ramps were carried out at a rate of 2 °C min^{-1} with an applied frequency of 10 rad s^{-1}. All experiments were carried out within the linear viscoelastic regime (LVE), as verified by strain sweep measurements from 0.01 to 100% for each sample. The crossover time ($\tau_{crossover}$) was determined from the intersection of the storage (G') and loss (G'') moduli and determined as $\tau_{crossover} = 1/\omega_{crossover}$. This criterion reflects the transition from a viscoelastic solid to liquid and the onset of flow in vitrimers. These relaxation times were plotted as a function of $1000/T$ and fit to an Arrhenius equation, from which the activation energy for flow was extracted from the slope. Strain sweep experiments were performed under large amplitude oscillatory shear (LAOS) flow. The samples were subjected to an increasing oscillatory strain from 0.01% to 100% in a ramp up step at 30 °C. Subsequently, a reverse strain sweep was conducted, decreasing the oscillatory strain from 100% back to 0.01% in a ramp down step to assess strain recovery.

Results & discussion

Impact of crosslink density on networks with fixed salt concentration

A series of transparent and flexible imine vitrimer electrolytes (VE) and neutral networks (V) were synthesized to systematically investigate the roles of crosslink density and salt concentration on viscoelasticity and conductivity (Fig. 1). The molecular weight of PEO was first varied (M_n = 1000, 2000 or 6000 g mol^{-1})

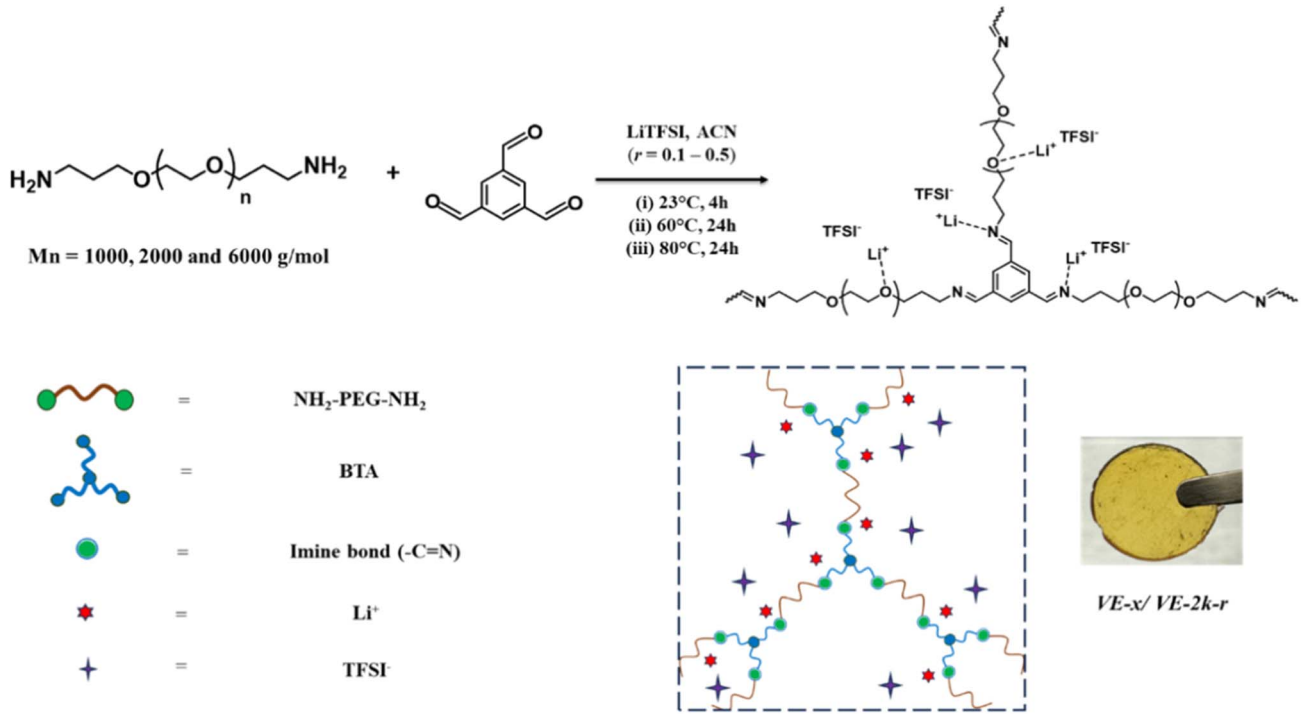

Fig. 1 Synthesis scheme for imine vitrimers. Poly(ethylene glycol) diamine and benzene-1,3,5-tricarbaldehyde undergo a Schiff-base reaction to form a telechelic imine network. The ratio between lithium salt and ethylene oxide repeat units is fixed at $r = 0.1$ to study the effect of crosslinking density on the viscoelasticity and ionic conductivity.

while maintaining a fixed $r = 0.1$. ATR-FTIR confirmed high conversion of vitrimer networks *via* the disappearance of the carbonyl (–C═O) peak, corresponding to the BTA crosslinker at 1695 cm^{-1}, and the appearance of the imine (–C═N–) peak at 1650 cm^{-1} with no observable excess amine ($–NH_2$) functionality. However, some small fraction of amine groups will exist below the FTIR detection limit. The broad peak at 2883 cm^{-1} corresponds to the (–C–H) stretching of PEO chains and peaks from 1100–1080 cm^{-1} were attributed to (–C–O–C) vibrational stretching in the PEO backbone (Fig. S1).

Thermogravimetric analysis (TGA) further confirmed high conversion as no water or volatile species leave the samples prior to degradation. All vitrimer networks and electrolytes show the onset of degradation (T_d) above 350 °C, indicating high stability at subsequent measurement temperatures (Fig. S4). DSC second heating curves showed the glass transition temperature (T_g) was −50 °C for all neutral networks, while the melting temperature (T_m) increased with linker length from 22 to 39 to 67 °C for V-1k, V-2k and V-6k networks, respectively (Fig. S2). Upon salt addition, the T_m peak disappeared and T_g values monotonically increased for all VE relative to V networks. All VE were amorphous, attributed to the interactions between Li ions and the PEO backbone disrupting crystallization, consistent with prior studies on salt-containing PEO.[24,72] T_g values further increase with higher crosslinking density reflecting the suppression of chain mobility.[6,73] (Table 1 and Fig. S3).

Table 1 Summary of thermal and viscoelastic characteristics of imine vitrimers with varying crosslinking density and salt addition[a]

Samples	T_g (°C)	T_m (°C)	T_d (°C)	$\tau_{130\ °C}$ (sec)	E_a (kJ mol^{-1})
V-1k	−50	22	366	1.56	45 ± 4
VE-1k	−32	—	389	0.18	70 ± 8
V-2k	−50	39	374	0.14	51 ± 4
VE-2k	−35	—	390	0.07	65 ± 9
V-6k	−50	67	375	0.10	56 ± 5
VE-6k	−39	—	393	0.54	65 ± 7

[a] Salt concentration was fixed at $r = 0.1$.

Viscoelastic properties of vitrimers and electrolytes were first measured as a function of varying crosslinking density with fixed salt addition ($r = 0.1$) and compared to their neutral analogs. Frequency sweep experiments were carried out on each sample in 10 °C intervals from 130 °C to 30 °C to measure the storage (G') and loss (G'') moduli as a function of frequency (Fig. S5 and S6). For all systems, a viscous flow regime at low frequency was observed at elevated temperatures but could not be clearly resolved at 30 °C. At higher frequency, the networks exhibited a rubbery plateau with $G' > G''$. As the crosslinking density increased, the plateau modulus at 130 °C increases from 0.25 to 2 MPa for neutral networks (Fig. 2a). In contrast, the G' values of the VE's are lower (0.1–1 MPa) compared to their salt-free counterparts (Fig. 2b). This reduction in G' is attributed to the plasticization effect of large $TFSI^-$ anions. Unlike linear PEO based solid electrolytes, both the neutral and salt-containing networks preserved their modulus with increasing temperatures even as bond exchange is accelerated.[74] (Fig. S7 and S8). Additionally, the hypothetical vitrimer topology freezing

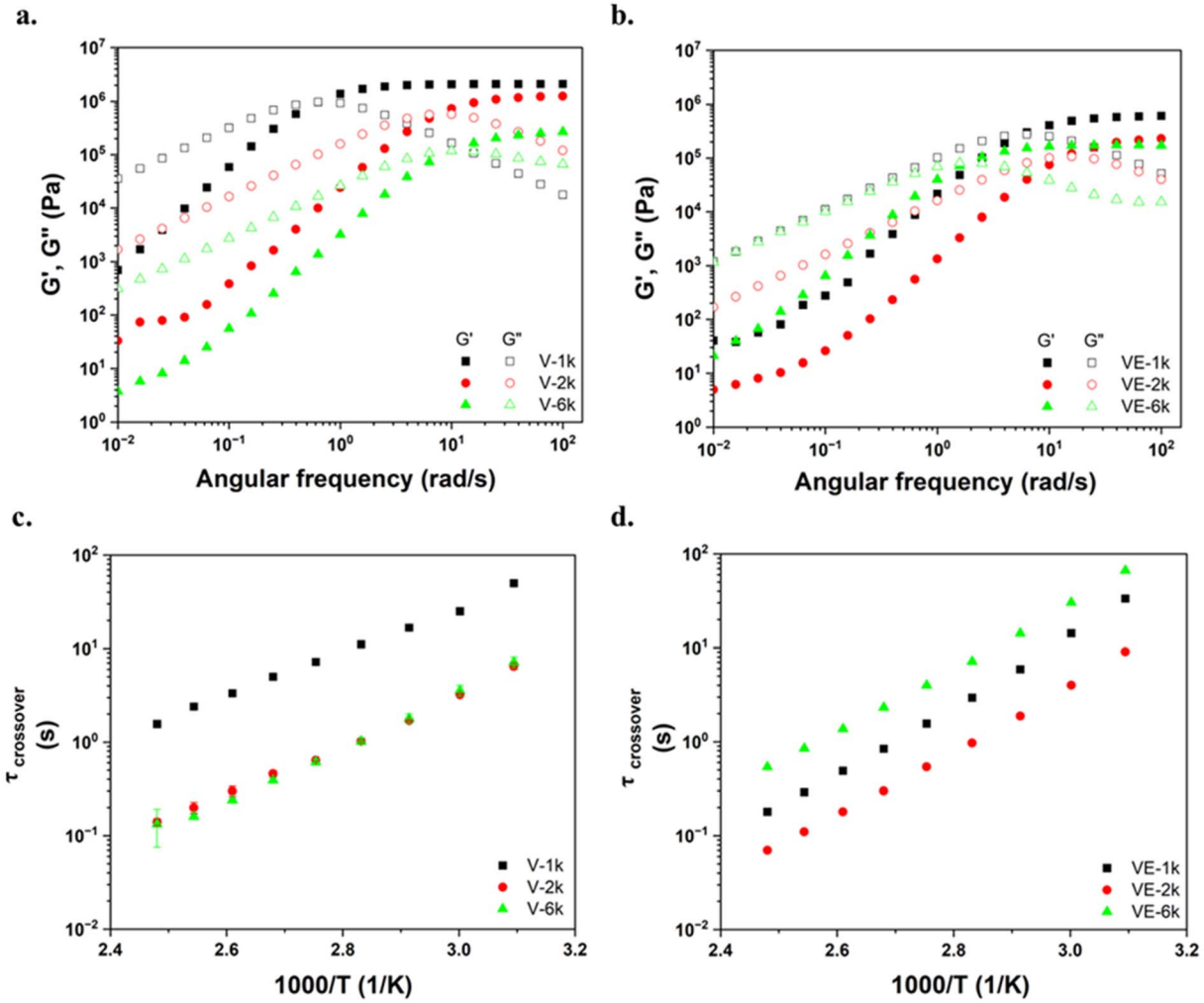

Fig. 2 Frequency sweep showing the modulus (G', solid symbols and G'', open symbols) as a function of angular frequency for (a) neutral networks (V) and (b) networks with salt (VE) at 130 °C. For both V and VE series, G' increases with increasing crosslinking density, indicating enhanced network stiffness. Arrhenius plots of $\tau_{crossover}$ as a function of inverse temperature (1000/T) for imine networks (c) without and (d) with salt show non-monotonic trends with linker length. Despite catalytic effect of salt addition on bond exchange, VE samples exhibit higher activation energies, relative to the V networks, indicating stronger temperature dependence of salt dissociation on exchange dynamics.

temperature (T_v) was estimated by extrapolating the viscosity η to 10^{12} Pa s[75] using the Maxwell relationship ($\eta = G \times \tau$) and frequency sweep data. The viscosity exhibits an Arrhenius temperature dependence as the network dynamics are governed by exchange reactions even at 30 °C, which is still 80 °C above T_g (Fig. S9). A T_v value of – 64 °C was obtained for VE-2k which is lower than T_g and not experimentally accessible. Extrapolation based on a higher temperature data will result in different T_v values compared to data near the glass transition.

The characteristic relaxation time ($\tau_{crossover}$) was plotted as a function of $1/T$ for different crosslink densities and revealed Arrhenius behavior with activation energies (E_a) of 45, 51 and 56 kJ mol^{-1} for V-1k, 2k and 6k networks, respectively (Table 1). These are in the typical range for imine vitrimers[76,77] but exhibit an opposite trend to prior telechelic networks with vinylogous urethane[50] and boronic ester[78] dynamic crosslinks, where E_a increased with crosslink density. Relaxation times in vitrimers are typically described by the Arrhenius equation $\tau = \tau_0 \exp(E_a/RT)$, while recent work[79] has proposed separate contributions from the exchange reaction and the segmental dynamics which impacts mobility of network components as:

$$\tau = A \exp\left(\frac{\Delta H_b}{RT}\right) + t_p \tau_\alpha(T)$$

The first term captures the exchange reaction with enthalpy barrier ΔH_b and a prefactor A related to the collision frequency of exchanging groups and steric effects when specific orientations are needed for the reaction. The second term is the alpha or segmental relaxation time ($\tau_\alpha(T)$) which govern mobility of network components and a prefactor t_p which is attributed to either chemistry specific effects or crosslinker mobility. Although $\tau_\alpha(T)$ is much smaller than the bulk τ, the prefactor t_p can apparently reach values of 10^5–10^7 in imine vitrimers. In the neutral vitrimers, T_g is invariant with linker length and the activation energy for imine exchange is assumed constant as the

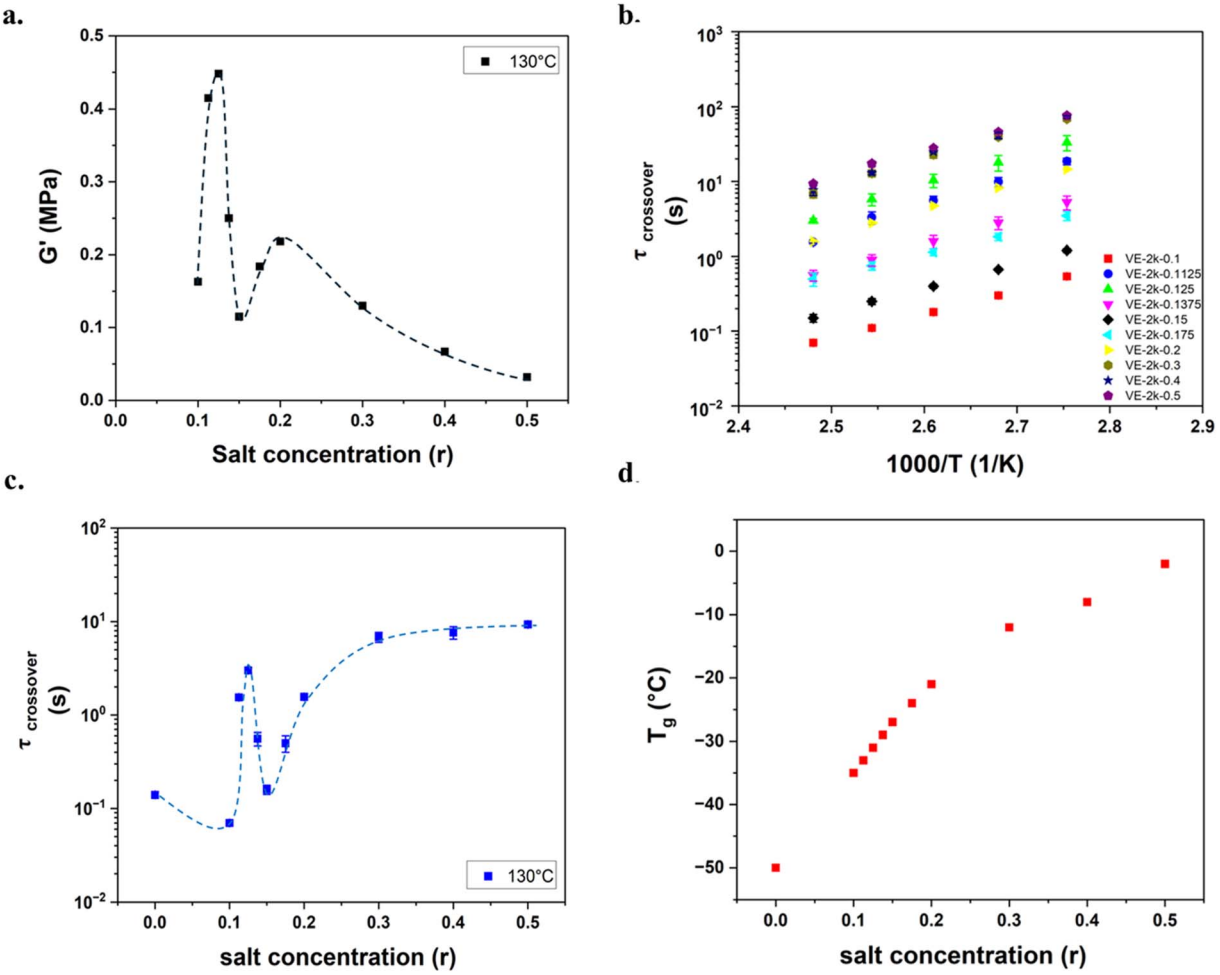

Fig. 3 (a) Plateau modulus (G') shows non-monotonic variation with increasing salt content at 130 °C. (b) $\tau_{crossover}$ plotted against inverse temperature (1000/T) shows Arrhenius behavior with no specific trend for Ea. (c) $\tau_{crossover}$ as a function of salt concentration shows a non-monotonic trend, where bond exchange dynamics slows down up to $r = 0.125$. It increases from $r = 0.1375$ to 0.15 and finally slows down and saturates at high salt concentration up to $r = 0.5$. (d) T_g increases monotonically with increasing salt, indicating that the increased T_g alone does not explain the trends in bond-exchange dynamics.

polymer chemistry does not change. The V-1k has the shortest linker lengths which reduces the distance over which imine groups must translate to exchange. However, the shortest chains are also the least flexible and may hinder the ability to form the required conformation for exchange. Analysis of the prefactor τ_0 from the simple Arrhenius equation decreases from $\sim 10^{-7}$ to 10^{-10} s as linker length goes from 1k to 6k. Thus, the imine bonds in V-1k can encounter more frequently but still exchange slower if their orientations are not suitable for the reaction. The (modestly) lower apparent E_a may be a convolution of how the chemical reaction and segmental dynamics change with temperature which is not explicitly accounted for and requires additional measurements of the alpha relaxation time. This counterintuitive response has also been observed in the case of telechelic vinylogous urethane networks.[47,80] The upturn upon cooling for V-6k is attributed to crystallinity which occurs below 50 °C (Fig. 2c).

A key finding of the present work is that addition of LiTFSI salt can either accelerate (VE-1k and VE-2k) or slow bulk relaxation (VE-6k) leading to an unexpected non-monotonic trend (Fig. 2d). The Li^+ cations coordinate with both ether oxygens in the chains and imine bonds to form transient crosslinks, which can increase the effective crosslinking density leading to slower bond exchange, especially in case of VE-6k. The E_a values are all higher for VEs compared to neutral networks and span a smaller range of 65–70 kJ mol^{-1} (Table 1). This is attributed to the temperature-dependence of salt dissociation, where more free Li^+ are expected to catalyze bond exchange at higher temperature and control the rate of exchange more than segmental dynamics or chain diffusion. The characteristic relaxation times do not superpose when plotted against normalized temperature T_g/T for V and VE series and retain the non-monotonic trend (Fig. S10).

These results are attributed to a complex interplay of bond exchange, linker/crosslinker diffusion, and salt dissociation which all have distinct temperature dependences and can impact the overall relaxation times. Future work is needed to capture these factors in a unified model.

Table 2 Summary of thermal and viscoelastic characteristics of imine vitrimers with varying salt concentrations

Samples	T_g (°C)	T_d (°C)	$\tau_{130\ °C}$ (sec)	E_a (kJ mol^{-1})
VE-2k-0.1	−35	390	0.1	65 ± 9
VE-2k-0.1125	−33	387	1.5	77 ± 7
VE-2k-0.125	−31	388	3.0	75 ± 11
VE-2k-0.1375	−29	391	0.6	68 ± 7
VE-2k-0.15	−27	386	0.2	62 ± 6
VE-2k-0.175	−24	393	0.5	59 ± 7
VE-2k-0.2	−21	391	1.6	68 ± 8
VE-2k-0.3	−12	394	6.8	68 ± 5
VE-2k-0.4	−8	391	7.7	63.75 ± 5
VE-2k-0.5	−2	387	9.3	63 ± 9

Impact of salt concentration at fixed linker length on viscoelasticity

Next, the role of salt concentration on the viscoelastic properties was examined at a fixed linker length of 2000 g mol^{-1} and as a function of temperature (Fig. S11). The electrolytes retain a G' above 10^5 Pa and exhibit a non-monotonic variation with salt concentration (Fig. 3a) with an initial increase from r = 0.1–0.125, decrease for r = 0.125–0.15, and then increase with further salt addition up to r = 0.2. At r = 0.4 and 0.5, the modulus then drops by an order of magnitude (10^4 − 10^5 Pa) due to increased plasticizing effect from the counterion TFSI$^-$. Similar to the variations in plateau modulus, a non-monotonic trend is also observed in crossover time as a function of increasing r at 130 °C, chosen to be well above T_g to minimize impacts of segmental dynamics and provide the fastest bond exchange (Fig. 3b, c and Table 2). Initially salt has a small catalytic effect for r = 0.1 relative to the neutral sample. From r = 0.1 to 0.125, $\tau_{crossover}$ increases from 0.07 s to 3 s, attributed to an increase in ion aggregation (discussed in the WAXS section). Next, $\tau_{crossover}$ decreases from r = 0.125–0.15 attributed to the catalytic effect of Li on bond exchange. Finally, increasing r further to 0.175 leads to slower $\tau_{crossover}$ and appears to saturate at salt concentrations above r = 0.3.

Despite the complex salt-dependence of $\tau_{crossover}$ and G', T_g exhibits a consistent upward trend with increasing salt concentration, a behavior commonly observed in polyether-based electrolytes[45,81,82] (Fig. 3d). Relaxation times do not collapse onto a single curve *versus* normalized temperature T_g/T. Only the r > 0.3 samples appear to overlap, and in this regime segmental dynamics play a more dominant role (Fig. S12). These findings indicate that salt concentration will impact the rate at which a VE can relax stresses during battery cycling or reconfigure in response to a roughening electrode surface.

As a proof of concept, VE-1k, 2k and 6k were also tested under large amplitude oscillatory shear deformation and demonstrated a strain invariant response at 30 °C (Fig. S13). The strain was first ramped up to 100%, then back down with minimal changes in the storage and loss moduli. This is in stark contrast to permanent network electrolytes which show an overshoot in loss modulus and drop in storage modulus at critical strains of 1–5%,[35] highlighting the broader potential of VEs for battery applications.

Impact of linker length and salt concentration on conductivity

Ionic conductivity was measured for vitrimer electrolytes as a function of varying crosslinking density and r = 0.1 from 130 °C to 30 °C in 10 °C increments. The conductivity increases monotonically with temperature, which is expected for ionic polymer electrolytes and has a non-Arrhenius dependence on temperature.[83–85] All samples are well described by the Vogel–Tammann–Fulcher (VTF) model, indicating that ion transport is coupled to the segmental dynamics (Fig. S14). The pre-exponential factor (σ_∞), which represents the limiting high temperature conductivity, exhibits a non-monotonic trend analogous to that observed in the measured ionic conductivity (Table S1). Ionic conductivities at 130 °C were 7 × 10^{-3}, 9.2 × 10^{-3} and 3.8 × 10^{-3} S cm^{-1} at 130 °C for VE-1k, VE-2k and VE-6k, respectively (Fig. 4a). The VE-2k electrolyte shows the highest conductivity, correlated with the faster bond exchange, and this system appears to have the optimal balance of EO and imine to promote salt dissociation for ion transport and bond exchange catalysis. Followed by this, VE-1k shows lower conductivity and slower $\tau_{crossover}$, while VE-6k was least conductive and had the longest relaxation times. We emphasize that faster bond exchange is not accelerating ionic conductivity as they occur on vastly different timescales, but rather both are due to greater salt dissociation. Ionic conductivity plots were not superimposed upon T_g normalization (Fig. 5a). All the samples show elevated ionic conductivity relative to a linear PEO/LiTFSI control attributed to the imine bonds which may improve LiTFSI salt dissociation.

Ionic conductivity was further evaluated as a function of varying salt concentration (r) over a broad temperature range (Fig. 4b). The VE-2k was chosen for this investigation as it exhibited both the fastest relaxation times and highest conductivities. All samples are fitted using the VTF model (Fig. S15). However, there is no discernible trend among VTF fit parameters with the varying salt concentration (Table S2). At 130 °C, a salt concentration of r = 0.1 yields the maximum ionic conductivity, followed by a non-monotonic trend with the same regimes as crossover times (Fig. 4c). Conductivity drops going to r = 0.125 (where $\tau_{crossover}$ increases) and then increases up to r = 0.15 (where $\tau_{crossover}$ decreases). Further salt addition up to r = 0.5 led to a continual decrease in conductivity (where $\tau_{crossover}$ is invariant). This non-monotonic trend is attributed to the dual role of free ions on conductivity and catalyzing bond exchange from r = 0.1–0.2. Higher salt concentration increases T_g, and both conductivity and $\tau_{crossover}$ reasonably collapse as a function of T_g/T (Fig. 5b and S12).

The intermediate concentrations of r = 0.1 to 0.2 are more difficult to explain, but a competition between interactions between Li and imine groups and increased salt aggregation are likely contributing. The advantage of the non-monotonic trends are that an intermediate salt concentration and linker length can optimize both high conductivity and fast bond exchange, while retaining a modulus greater than 10^5 Pa. This has implications for improved cycling as the electrolyte can reconfigure at the electrode as shown in recent work.[86]

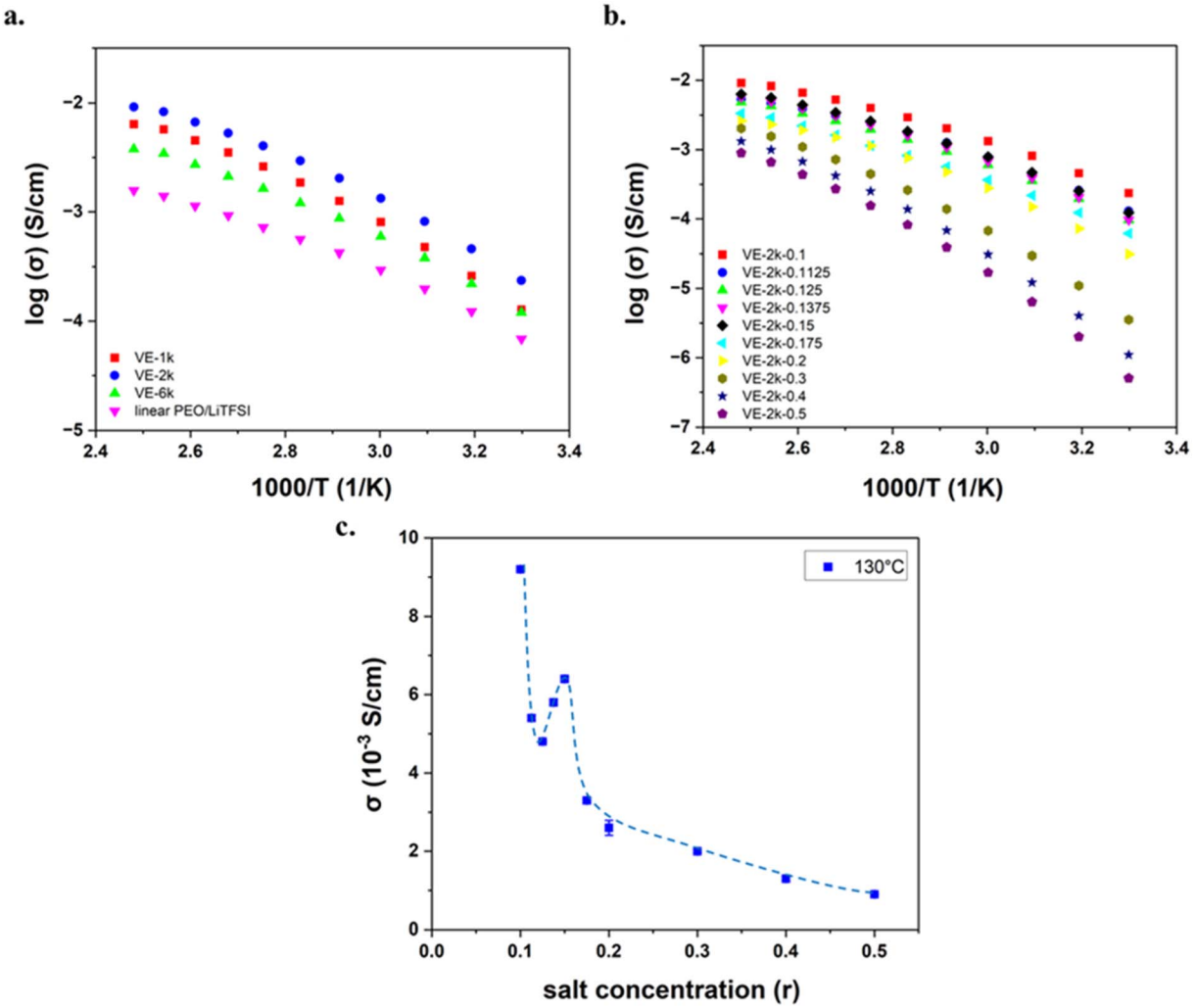

Fig. 4 (a) Temperature-dependent ionic conductivity of imine vitrimer electrolytes (VE-*x*) compared to linear PEO/LiTFSI control from 130 °C to 30 °C. VE-2k sample shows the highest ionic conductivity (b) effect of salt concentration on the ionic conductivity of VE-2k electrolytes. (c) Similar to bond exchange dynamics, non-monotonic behavior is also observed for σ with increasing r values. Even at higher salt loadings of $r =$ 0.5, ionic conductivity of 9×10^{-4} S cm^{-1} is observed at 130 °C, demonstrating good electrochemical performance.

WAXS and NMR investigations of aggregation and Li partitioning

To probe the extent of ion aggregation with increasing salt concentration, Wide-Angle X-ray Scattering (WAXS) was performed (Fig. S16). An anion–anion correlation peak appears at $q = 9.5$ nm^{-1} and the intensity varies with increasing r (Fig. 6). From $r = 0.1$ to 0.125, the intensity of the peak becomes stronger which is consistent with fewer free ions to catalyze bond exchange or lead to conductivity. When r is increased further to 0.15, the peak intensity decreases suggesting a lower degree of ionic aggregation. The ionic aggregates are spatially less correlated, allowing improved salt dissociation and ionic mobility which is increasingly decoupled from segmental dynamics. From $r = 0.175$–0.2, the intensity increases again corresponding to decreasing ionic conductivity and slower relaxation time. At the highest salt loadings ($r > 0.2$), aggregation continually decreased while conductivity and modulus decrease and $\tau_{crossover}$ exhibited a plateau. This indicates that the high salt regime is no longer directly correlated with the ionic aggregate peak, but rather the increased T_g. The electrolytes remain optically transparent up to $r = 0.5$, indicating that no salt-induced crystallization occurred (Fig. S17). In linear PEO, phase separation has been reported above $r = 0.28$.[71]

The local environment for Li cations was probed using ^{7}Li solid-state NMR (ssNMR) on samples with varying salt concentrations $r = 0.1$–0.5 (Fig. 7). ^{7}Li ssNMR has been previously employed to examine the interactions between lithium ions with the ether oxygens of ethylene oxide and coordinates with the vinylogous urethane and boronic ester dynamic bonds.[45,46,50] As reference materials, a small molecule *N*-benzylidenebenzylamine (no EO present) was mixed with 10 mol% LiTFSI salt (Li-Im) and showed a chemical shift of −0.05 ppm. A mixture of LiTFSI salt and diethylene glycol ethyl ether (DEG) served as a small-molecule PEO analogue (Li-EO) and previous studies[50] reported a chemical shift of −1.4 ppm. The network electrolytes were then measured as a function of increasing salt concentration and in all cases were intermediate to the pure Li-

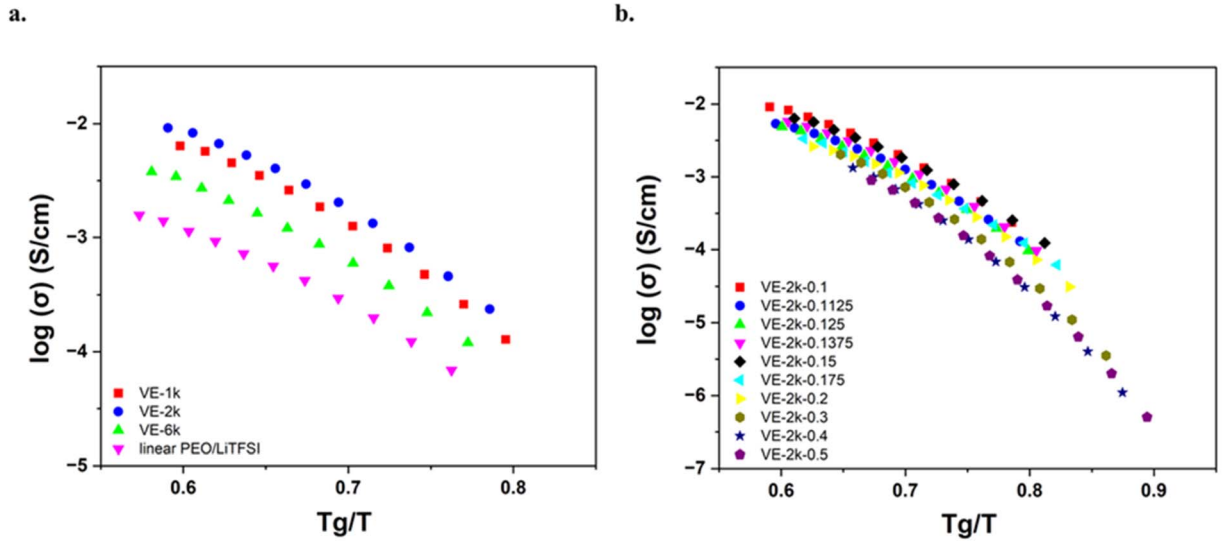

Fig. 5 (a) Comparison of T_g-normalized temperature-dependent conductivities for networks with varying crosslinking density at a fixed LiTFSI concentration ($r = 0.1$). (b) Plot of ionic conductivity *versus* T_g-normalized temperature for networks with 2000 g mol^{-1} -EO chains across all investigated r values. Both indicate that ion transport is decoupled from segmental dynamics and temperature dependence of imine bond exchange.

EO and Li-Im systems. The $r = 0.1$ system had a chemical shift of −0.9 ppm and was closest to the Li-Im compound. Increasing the concentration to $r = 0.125$ lead to a pronounced downward shift of 0.25 ppm to −1.15 ppm. Further salt addition did not substantially change the chemical shift up to $r = 0.4$, but at $r = 0.5$ a further downfield shift to −1.25 ppm was observed. In contrast to the non-monotonic variation observed in the WAXS ion aggregate peak intensity, the ^{7}Li NMR spectra shows no appreciable change in chemical shift and the Li environment is similar to pure LiTFSI salt and is likely reflecting nearest neighbor interactions at concentrations $r = 0.125$–0.4. ^{7}Li NMR is primarily sensitive to the local coordination environment of Li^+ rather than to the longer range degree of ionic aggregation measured by WAXS. The nearly invariant chemical shift suggests that Li^+ continues to reside in a similar first coordination shell, predominantly interacting with ether oxygens, imine groups, and $TFSI^-$ anions, even as the organization of ionic aggregates evolves. At $r = 0.5$ the NMR signal shifts slightly closer to the −1.4 ppm value for the Li-EO reference. The broadening of peaks observed with increasing salt

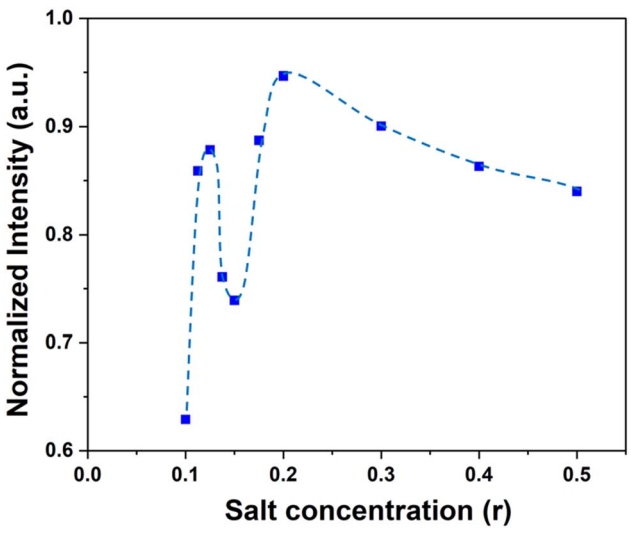

Fig. 6 Normalized intensity plot for VE-2k electrolytes with varying salt concentrations, obtained from Wide-angle X-ray Scattering (WAXS). WAXS analysis supports the non-monotonic trends in bond-exchange dynamics and ionic conductivity, as evident by change in the intensity of peak at $q = 9.5$ nm^{-1}, corresponding to ion aggregation.

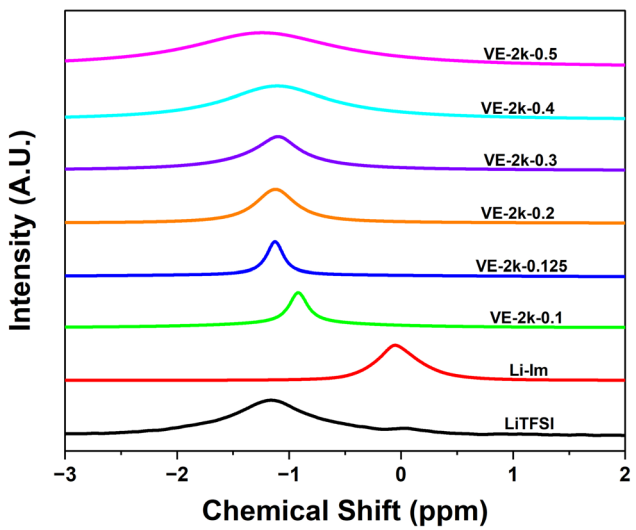

Fig. 7 ^{7}Li solid-state NMR illustrating the effect of varying salt concentrations on the coordination of Li^+ cations with the ether oxygens of ethylene oxide repeat units and imine dynamic bond sites. Increasing the concentration of Li salt in the electrolyte leads to a pronounced downward shift of the ^{7}Li NMR peaks indicating enhanced shielding of Li ions, which makes them ineffective in catalyzing bond exchange.

concentration is due to lower Li mobility and the higher T_g of these samples all measured at room temperature.

Conclusion

Conductivity and viscoelasticity of imine vitrimer electrolytes with varying crosslinking density and salt concentration were systematically investigated. The $\tau_{crossover}$ and ionic conductivity values reveal a complex, non-monotonic trend as a function of crosslinking density (with fixed salt) or r (at fixed crosslink density). Despite lowest crosslinking density and T_g, the VE-6k sample shows the slowest bond exchange and lowest ionic conductivity at $r = 0.1$. For VE-2k at $r = 0.1$–0.2, three distinct regimes are observed in conductivity, modulus, and relaxation times. WAXS indicates that these trends are closely correlated with ion aggregation peak, as a weaker scattering intensity corresponds to faster relaxation, higher conductivity, and lower modulus. No evidence of salt-induced crystallization is observed even up to $r = 0.5$, higher than in linear PEO. The amorphous morphology leads to enhanced conductivity relative to linear PEO while retaining plateau moduli $>10^5$ Pa. These results highlight the complexity of how the bulk viscoelasticity and conductivity depend on salt in vitrimer electrolytes and provide new insights on the key role of salt aggregation. Future directions include plasticized VEs with enhanced conductivities at lower temperatures relevant to battery applications, as well as the impact of polar small molecules on bond exchange. Such insights are important for designing the next-generation of vitrimer electrolytes with diverse dynamic bond or backbone chemistries.

Conflicts of interest

The authors declare no competing financial interest.

Data availability

The data supporting the findings of this study are included in the main text and supplementary information (SI). Supplementary information: FTIR spectra; DSC; TGA; rheological characterization of neutral networks (V-x) and vitrimer electrolytes (VE-x) with varying crosslinking density as a function of angular frequency; shear modulus of (V-x) and (VE-x) as a function of increasing temperature; crossover times *vs.* normalized temperature (T_g/T); rheological characterization of vitrimer electrolytes with fixed crosslinking density and varying salt concentration (VE-2k-r) as a function of angular frequency; crossover times of VEs with varying r as a function of normalized temperature (T_g/T); WAXS; Image of VE-2k-0.5 vitrimer electrolyte showing transparency and no sign of salt-induced crystallization. See DOI: https://doi.org/10.1039/d6ta00316h.

Acknowledgements

This project was supported by the Toyota Research Institute of North America (TRINA). We gratefully acknowledge the use of research facilities at the Material Research Laboratory and School of Chemical Sciences NMR Laboratory at UIUC.

References

1 *Topics > Lithium-Ion Battery Industry Worldwide*, https://www.statista.com/chart/23808/lithium-ion-battery-demand/2/8.
2 J. B. Goodenough, How We Made the Li-Ion Rechargeable Battery: Progress in Portable and Ubiquitous Electronics Would Not Be Possible without Rechargeable Batteries. John B. Goodenough Recounts the History of the Lithium-Ion Rechargeable Battery, *Nat. Electron.*, 2018, 204, DOI: 10.1038/s41928-018-0048-6.
3 S. Yang, S. Park, S. Kim and S. K. Kim, Vitrimer with Dynamic Imine Bonds as a Solid-State Electrolyte for Lithium Metal Batteries, *Mater. Today Energy*, 2024, **45**, 101690, DOI: 10.1016/j.mtener.2024.101690.
4 D. Bresser, K. Hosoi, D. Howell, H. Li, H. Zeisel, K. Amine and S. Passerini, Perspectives of Automotive Battery R&D in China, Germany, Japan, and the USA, *J. Power Sources*, 2018, **382**, 176–178, DOI: 10.1016/j.jpowsour.2018.02.039.
5 F. Zheng, M. Kotobuki, S. Song, M. O. Lai and L. Lu, Review on Solid Electrolytes for All-Solid-State Lithium-Ion Batteries, *J. Power Sources*, 2018, **389**, 198–213, DOI: 10.1016/j.jpowsour.2018.04.022.
6 Q. Zhao, S. Stalin, C. Z. Zhao and L. A. Archer, Designing Solid-State Electrolytes for Safe, Energy-Dense Batteries. Nature Reviews Materials, *Nat. Res.*, 2020, **1**, 229–252, DOI: 10.1038/s41578-019-0165-5.
7 J.-M. Tarascon and M. Armand, *Issues and Challenges Facing Rechargeable Lithium Batteries*, 2001, https://www.nature.com.
8 J. B. Goodenough and K. S. Park, The Li-Ion Rechargeable Battery: A Perspective, *J. Am. Chem. Soc.*, 2013, **30**, 1167–1176, DOI: 10.1021/ja3091438.
9 B. Liu, J. G. Zhang and W. Xu, Advancing Lithium Metal Batteries, *Joule*, 2018, 833–845, DOI: 10.1016/j.joule.2018.03.008.
10 X. B. Cheng, C. Z. Zhao, Y. X. Yao, H. Liu and Q. Zhang, Recent Advances in Energy Chemistry between Solid-State Electrolyte and Safe Lithium-Metal Anodes, *Chem*, 2019, **10**, 74–96, DOI: 10.1016/j.chempr.2018.12.002.
11 S. Yang, S. Park, S. Kim and S. K. Kim, Vitrimer with Dynamic Imine Bonds as a Solid-State Electrolyte for Lithium Metal Batteries, *Mater. Today Energy*, 2024, **45**, 101690, DOI: 10.1016/j.mtener.2024.101690.
12 S. Xia, X. Wu, Z. Zhang, Y. Cui and W. Liu, *Practical Challenges and Future Perspectives of All-Solid-State Lithium-Metal Batteries*, Chem. Elsevier Inc., 2019, pp. 753–785, DOI: 10.1016/j.chempr.2018.11.013.
13 R. Chen, Q. Li, X. Yu, L. Chen and H. Li, Approaching Practically Accessible Solid-State Batteries: Stability Issues Related to Solid Electrolytes and Interfaces, *Chem. Rev.*, 2020, **22**, 6820–6877, DOI: 10.1021/acs.chemrev.9b00268.
14 K. Deng, Q. Zeng, D. Wang, Z. Liu, G. Wang, Z. Qiu, Y. Zhang, M. Xiao and Y. Meng, Nonflammable Organic Electrolytes for High-Safety Lithium-Ion Batteries, *Energy Storage Mater.*, 2020, 425–447, DOI: 10.1016/j.ensm.2020.07.018.

15 H. Li, J. Yang, S. Chen, Z. Xu, J. Wang, Y. Nuli, Y. Guo and C. Liang, Inherently Flame-Retardant Solid Polymer Electrolyte for Safety-Enhanced Lithium Metal Battery, *Chem. Eng. J.*, 2021, **410**, DOI: 10.1016/j.cej.2021.128415.
16 H. Jia, H. Onishi, N. von Aspern, U. Rodehorst, K. Rudolf, B. Billmann, R. Wagner, M. Winter and I. Cekic-Laskovic, A Propylene Carbonate Based Gel Polymer Electrolyte for Extended Cycle Life and Improved Safety Performance of Lithium Ion Batteries, *J. Power Sources*, 2018, **397**, 343–351, DOI: 10.1016/j.jpowsour.2018.07.039.
17 R. Schmitz, R. Schmitz, R. Müller, O. Kazakova, N. Kalinovich, G. V. Röschenthaler, M. Winter, S. Passerini and A. Lex-Balducci, Methyl Tetrafluoro-2-(Methoxy) Propionate as Co-Solvent for Propylene Carbonate-Based Electrolytes for Lithium-Ion Batteries, *J. Power Sources*, 2012, **205**, 408–413, DOI: 10.1016/j.jpowsour.2012.01.027.
18 N. Wang, Y. Wei, S. Yu, W. Zhang, X. Huang, B. Fan, H. Yuan and Y. Tan, A Flexible PEO-Based Polymer Electrolyte with Cross-Linked Network for High-Voltage All Solid-State Lithium-Ion Battery, *J. Mater. Sci. Technol.*, 2024, **183**, 206–214, DOI: 10.1016/j.jmst.2023.10.005.
19 Y. Guo, X. Qu, Z. Hu, J. Zhu, W. Niu and X. Liu, Highly Elastic and Mechanically Robust Polymer Electrolytes with High Ionic Conductivity and Adhesiveness for High-Performance Lithium Metal Batteries, *J. Mater. Chem. A*, 2021, **9**(23), 13597–13607, DOI: 10.1039/d1ta02579a.
20 A. Naboulsi, R. Chometon, F. Ribot, G. Nguyen, O. Fichet and C. Laberty-Robert, Correlation between Ionic Conductivity and Mechanical Properties of Solid-like PEO-Based Polymer Electrolyte, *ACS Appl. Mater. Interfaces*, 2024, **16**(11), 13869–13881, DOI: 10.1021/acsami.3c19249.
21 Z. Li, J. Fu, X. Zhou, S. Gui, L. Wei, H. Yang, H. Li and X. Guo, Ionic Conduction in Polymer-Based Solid Electrolytes, *Adv. Sci.*, 2023, **10**, e2201718, DOI: 10.1002/advs.202201718.
22 Z. Xue, D. He and X. Xie, Poly(Ethylene Oxide)-Based Electrolytes for Lithium-Ion Batteries, *J. Mater. Chem. A*, 2015, **17**, 19218–19253, DOI: 10.1039/c5ta03471j.
23 P. Bennington, C. Deng, D. Sharon, M. A. Webb, J. J. de Pablo, P. F. Nealey and S. N. Patel, Role of Solvation Site Segmental Dynamics on Ion Transport in Ethylene-Oxide Based Side-Chain Polymer Electrolytes, *J. Mater. Chem. A*, 2021, **9**(15), 9937–9951, DOI: 10.1039/d1ta00899d.
24 O. Borodin and G. D. Smith, Mechanism of Ion Transport in Amorphous Poly(Ethylene Oxide)/LiTFSI from Molecular Dynamics Simulations, *Macromolecules*, 2006, **39**(4), 1620–1629, DOI: 10.1021/ma052277v.
25 J. Mindemark, M. J. Lacey, T. Bowden and D. Brandell, Beyond PEO—Alternative Host Materials for Li+-Conducting Solid Polymer Electrolytes, *Progress in Polymer Science*, Elsevier Ltd June 1, 2018, pp. 114–143, DOI: 10.1016/j.progpolymsci.2017.12.004.
26 S. Xu, Z. Sun, C. Sun, F. Li, K. Chen, Z. Zhang, G. Hou, H. M. Cheng and F. Li, Homogeneous and Fast Ion Conduction of PEO-Based Solid-State Electrolyte at Low Temperature, *Adv. Funct. Mater.*, 2020, **30**(51), DOI: 10.1002/adfm.202007172.
27 S. Yan, Z. Wang, F. Liu, H. Zhou and K. Liu, Aromatic Donor–Acceptor Charge-Transfer Interactions Reinforced Supramolecular Polymer Electrolyte for Solid-State Lithium Batteries, *Adv. Funct. Mater.*, 2023, **33**(52), DOI: 10.1002/adfm.202303739.
28 H. Ben youcef, O. Garcia-Calvo, N. Lago, S. Devaraj and M. Armand, Cross-Linked Solid Polymer Electrolyte for All-Solid-State Rechargeable Lithium Batteries, *Electrochim. Acta*, 2016, **220**, 587–594, DOI: 10.1016/j.electacta.2016.10.122.
29 Y. Zhang, W. Lu, L. Cong, J. Liu, L. Sun, A. Mauger, C. M. Julien, H. Xie and J. Liu, Cross-Linking Network Based on Poly(Ethylene Oxide): Solid Polymer Electrolyte for Room Temperature Lithium Battery, *J. Power Sources*, 2019, **420**, 63–72, DOI: 10.1016/j.jpowsour.2019.02.090.
30 R. Khurana, J. L. Schaefer, L. A. Archer and G. W. Coates, Suppression of Lithium Dendrite Growth Using Cross-Linked Polyethylene/Poly(Ethylene Oxide) Electrolytes: A New Approach for Practical Lithium-Metal Polymer Batteries, *J. Am. Chem. Soc.*, 2014, **136**(20), 7395–7402, DOI: 10.1021/ja502133j.
31 S. Brox, S. Röser, T. Husch, S. Hildebrand, O. Fromm, M. Korth, M. Winter and I. Cekic-Laskovic, Alternative Single-Solvent Electrolytes Based on Cyanoesters for Safer Lithium-Ion Batteries, *ChemSusChem*, 2016, **9**(13), 1704–1711, DOI: 10.1002/cssc.201600369.
32 S. Feng, D. Shi, F. Liu, L. Zheng, J. Nie, W. Feng, X. Huang, M. Armand and Z. Zhou, Single Lithium-Ion Conducting Polymer Electrolytes Based on Poly[(4-Styrenesulfonyl)(Trifluoromethanesulfonyl)Imide] Anions, *Electrochim. Acta*, 2013, **93**, 254–263, DOI: 10.1016/j.electacta.2013.01.119.
33 X. Li, S. Liu, J. Shi, M. Huang, Z. Shi, H. Wang and Z. Yan, Poly (Ethylene Oxide) Based Solid Polymer Electrolyte Improved by Multifunctional Additives of Poly (Acrylamide) and LiI, *Electrochim. Acta*, 2023, **445**, 142062, DOI: 10.1016/j.electacta.2023.142062.
34 N. S. Wanakule, A. Panday, S. A. Mullin, E. Gann, A. Hexemer and N. P. Balsara, Ionic Conductivity of Block Copolymer Electrolytes in the Vicinity of Order-Disorder and Order-Order Transitions, *Macromolecules*, 2009, **42**(15), 5642–5651, DOI: 10.1021/ma900401a.
35 S. N. Chordia, P. V. Braun, S. N. Joshi, T. S. Arthur and C. M. Evans, Crosslinking Density and Salt Addition Impacts on the Large Amplitude Oscillatory Shear Response of Acrylate Network Electrolytes, *J. Polym. Sci.*, 2025, **63**(12), 2670–2679, DOI: 10.1002/pol.20250310.
36 X. Liu, L. Liang, M. Lu, X. Song, H. Liu and G. Chen, Water-Resistant Bio-Based Vitrimers Based on Dynamic Imine Bonds: Self-Healability, Remodelability and Ecofriendly Recyclability, *Polymer*, 2020, **210**, 123030, DOI: 10.1016/j.polymer.2020.123030.
37 H. Memon, Y. Wei, L. Zhang, Q. Jiang and W. Liu, An Imine-Containing Epoxy Vitrimer with Versatile Recyclability and Its Application in Fully Recyclable Carbon Fiber Reinforced Composites, *Compos. Sci. Technol.*, 2020, **199**, 108314, DOI: 10.1016/j.compscitech.2020.108314.

38 A. Liguori and M. Hakkarainen, Designed from Biobased Materials for Recycling: Imine-Based Covalent Adaptable Networks, *Macromol. Rapid Commun.*, 2022, **1**, DOI: 10.1002/marc.202100816.

39 T. D. Martins, M. T. Viciosa, M. B. Oliveira, A. Fernandes, J. F. Mano, C. Baleizão and J. P. S. Farinha, Reversible Imine Crosslinking in Waterborne Self-Healing Polymer Coatings, *Prog. Org. Coat.*, 2023, **180**, DOI: 10.1016/j.porgcoat.2023.107552.

40 K. Liang, G. Zhang, J. Zhao, L. Shi, J. Cheng and J. Zhang, Malleable, Recyclable, and Robust Poly(Amide-Imine) Vitrimers Prepared through a Green Polymerization Process, *ACS Sustain. Chem. Eng.*, 2021, **9**(16), 5673–5683, DOI: 10.1021/acssuschemeng.1c00626.

41 J. M. D. Lehn, Dynamic Molecular and Supramolecular Polymers, *Prog. Polym. Sci.*, 2005, **30**, 814–831, DOI: 10.1016/j.progpolymsci.2005.06.002.

42 U. O. I. U. Champaign and L. E. Biology, *Dynamers: Polyacylhydrazone Reversible Covalent Polymers, Component Exchange, and Constitutional Diversity*, 2004, vol. **101**, https://www.pnas.org.

43 Y. Ding, R. Miao, J. Liu, Z. Xin and C. Bao, Covalent Adaptable Networks Containing Nitrogen-Coordinated Boronic Ester and Imine Bonds, *ACS Appl. Polym. Mater.*, 2024, **6**(15), 9008–9016, DOI: 10.1021/acsapm.4c01334.

44 J. J. Cash, T. Kubo, D. J. Dobbins and B. S. Sumerlin, Maximizing the Symbiosis of Static and Dynamic Bonds in Self-Healing Boronic Ester Networks, *Polym. Chem.*, 2018, **9**(15), 2011–2020, DOI: 10.1039/c8py00123e.

45 B. B. Jing and C. M. Evans, Catalyst-Free Dynamic Networks for Recyclable, Self-Healing Solid Polymer Electrolytes, *J. Am. Chem. Soc.*, 2019, **141**(48), 18932–18937, DOI: 10.1021/jacs.9b09811.

46 B. B. Jing, P. Mata, Q. Zhao and C. M. Evans, Effects of Crosslinking Density and Lewis Acidic Sites on Conductivity and Viscoelasticity of Dynamic Network Electrolytes, *J. Polym. Sci.*, 2021, **59**(21), 2492–2501, DOI: 10.1002/pol.20210207.

47 Y. Lin, Y. Chen, Z. Yu, Z. Huang, J. C. Lai, J. B. H. Tok, Y. Cui and Z. Bao, Reprocessable and Recyclable Polymer Network Electrolytes *via* Incorporation of Dynamic Covalent Bonds, *Chem. Mater.*, 2022, **34**(5), 2393–2399, DOI: 10.1021/acs.chemmater.1c04396.

48 W. Denissen, M. Droesbeke, R. Nicola, L. Leibler, J. M. Winne and F. E. Du Prez, Chemical Control of the Viscoelastic Properties of Vinylogous Urethane Vitrimers, *Nat. Commun.*, 2017, **8**, DOI: 10.1038/ncomms14857.

49 L. Bai and J. R. Zheng, Reprocessable and Shape-Memory Vinylogous Urethane Vitrimer Composites Enhanced by Sacrificial and Self-Catalysis Zn(II)–Ligand Bonds, *Compos. Sci. Technol.*, 2020, **190**, DOI: 10.1016/j.compscitech.2020.108062.

50 S. Jang, E. I. Hernandez Alvarez, C. Chen, B. B. Jing, C. Shen, P. V. Braun, A. Schleife, C. M. Schroeder and C. M. Evans, Control of Lithium Salt Partitioning, Coordination, and Solvation in Vitrimer Electrolytes, *Chem. Mater.*, 2023, **35**(19), 8039–8049, DOI: 10.1021/acs.chemmater.3c01353.

51 M. Kathan, P. Kovaříček, C. Jurissek, A. Senf, A. Dallmann, A. F. Thünemann and S. Hecht, Kontrolle Der Kinetik von Iminaustauschreaktionen Mit Photoschaltern Zur Lichtgesteuerten Modulation Der Selbstheilung in Polysiloxannetzwerken, *Angew. Chem.*, 2016, **128**(44), 14086–14090, DOI: 10.1002/ange.201605311.

52 W. Gu, F. Li, T. Liu, S. Gong, Q. Gao, J. Li and Z. Fang, Recyclable, Self-Healing Solid Polymer Electrolytes by Soy Protein-Based Dynamic Network, *Advanced Science*, 2022, **9**(11), DOI: 10.1002/advs.202103623.

53 S. K. Schoustra, T. Groeneveld and M. M. J. Smulders, The Effect of Polarity on the Molecular Exchange Dynamics in Imine-Based Covalent Adaptable Networks, *Polym. Chem.*, 2021, **12**(11), 1635–1642, DOI: 10.1039/d0py01555e.

54 G. M. Scheutz, J. J. Lessard, M. B. Sims and B. S. Sumerlin, Adaptable Crosslinks in Polymeric Materials: Resolving the Intersection of Thermoplastics and Thermosets, *J. Am. Chem. Soc.*, 2019, **16**, 16181–16196, DOI: 10.1021/jacs.9b07922.

55 M. Ciaccia and S. Di Stefano, Mechanisms of Imine Exchange Reactions in Organic Solvents, *Org. Biomol. Chem.*, 2015, **21**, 646–654, DOI: 10.1039/c4ob02110j.

56 A. Chao, I. Negulescu and D. Zhang, Dynamic Covalent Polymer Networks Based on Degenerative Imine Bond Exchange: Tuning the Malleability and Self-Healing Properties by Solvent, *Macromolecules*, 2016, **49**(17), 6277–6284, DOI: 10.1021/acs.macromol.6b01443.

57 P. Chakma and D. Konkolewicz, Dynamic Covalent Bonds in Polymeric Materials, *Angew. Chem.*, 2019, **131**(29), 9784–9797, DOI: 10.1002/ange.201813525.

58 K. Deng, S. Zhou, Z. Xu, M. Xiao and Y. Meng, A High Ion-Conducting, Self-Healing and Nonflammable Polymer Electrolyte with Dynamic Imine Bonds for Dendrite-Free Lithium Metal Batteries, *Chem. Eng. J.*, 2022, **428**, DOI: 10.1016/j.cej.2021.131224.

59 J. M. D. Lehn, Dynamic Molecular and Supramolecular Polymers, *Prog. Polym. Sci.*, 2005, **30**, 814–831, DOI: 10.1016/j.progpolymsci.2005.06.002.

60 S. H. Lee, S. R. Shin and D. S. Lee, Self-Healing of Cross-Linked PU *via* Dual-Dynamic Covalent Bonds of a Schiff Base from Cystine and Vanillin, *Mater. Des.*, 2019, **172**, DOI: 10.1016/j.matdes.2019.107774.

61 L. Wan, X. Cao, X. Xue, Y. Tong, S. Ci, H. Huang and D. Zhou, Self-Healing and Flexible Ionic Gel Polymer Electrolyte Based on Reversible Bond for High-Performance Lithium Metal Batteries, *Energy Technol.*, 2022, **10**(2), DOI: 10.1002/ente.202100749.

62 X. Cao, P. Zhang, N. Guo, Y. Tong, Q. Xu, D. Zhou and Z. Feng, Self-Healing Solid Polymer Electrolyte Based on Imine Bonds for High Safety and Stable Lithium Metal Batteries, *RSC Adv.*, 2021, **11**(5), 2985–2994, DOI: 10.1039/d0ra10035h.

63 W. Zou, B. Jin, Y. Wu, H. Song, Y. Luo, F. Huang, J. Qian, Q. Zhao and T. Xie, *Light-Triggered Topological Programmability in a Dynamic Covalent Polymer Network*, 2020, vol. 6, https://www.science.org.

64 Z. Zou; C. Zhu; Y. Li; X. Lei; W. Zhang; J. R. Xiao, *Fully Recyclable, and Malleable Electronic Skin Enabled by*

Dynamic Covalent Thermoset Nanocomposite; 2018. https://www.science.org.

65 Z. Q. Lei, P. Xie, M. Z. Rong and M. Q. Zhang, Catalyst-Free Dynamic Exchange of Aromatic Schiff Base Bonds and Its Application to Self-Healing and Remolding of Crosslinked Polymers, *J. Mater. Chem. A*, 2015, **3**(39), 19662–19668, DOI: 10.1039/c5ta05788d.

66 L. Zhang, P. Zhang, C. Chang, W. Guo, Z. H. Guo and X. Pu, Self-Healing Solid Polymer Electrolyte for Room-Temperature Solid-State Lithium Metal Batteries, *ACS Appl. Mater. Interfaces*, 2021, **13**(39), 46794–46802, DOI: 10.1021/acsami.1c14462.

67 S. Yang, S. Park, S. Kim and S. K. Kim, Vitrimer with Dynamic Imine Bonds as a Solid-State Electrolyte for Lithium Metal Batteries, *Mater. Today Energy*, 2024, **45**, DOI: 10.1016/j.mtener.2024.101690.

68 S. Lascaud, M. Perrier, A. Vallée, S. Besner, J. Prud'homme and M. Armand, *Phase Diagrams and Conductivity Behavior of Poly(Ethylene Oxide)-Molten Salt Rubbery Electrolytes Introduction Thin-Film Polyether Electrolytes Have Opened a Route*, 1994, vol. 27, https://pubs.acs.org/sharingguidelines.

69 M. Marzantowicz, F. Krok, J. R. Dygas, Z. Florjańczyk and E. Zygadło-Monikowska, The Influence of Phase Segregation on Properties of Semicrystalline PEO:LiTFSI Electrolytes, *Solid State Ionics*, 2008, **179**(27–32), 1670–1678, DOI: 10.1016/j.ssi.2007.11.035.

70 M. Chintapalli, T. N. P. Le, N. R. Venkatesan, N. G. Mackay, A. A. Rojas, J. L. Thelen, X. C. Chen, D. Devaux and N. P. Balsara, Structure and Ionic Conductivity of Polystyrene-Block-Poly(Ethylene Oxide) Electrolytes in the High Salt Concentration Limit, *Macromolecules*, 2016, **49**(5), 1770–1780, DOI: 10.1021/acs.macromol.5b02620.

71 L. S. Grundy, S. Fu, Z. J. Hoffman and N. P. Balsara, Electrochemical Characterization of PEO/LiTFSI Electrolytes Near the Solubility Limit, *Macromolecules*, 2022, **55**(20), 9030–9038, DOI: 10.1021/acs.macromol.2c01655.

72 H. M. Nekoomanesh, N. Shin-ichi, C. Booth and J. R. Owen, The Effect of Oxyethylene Sequence Length on the Properties of Poly [oxymethylene - oligo(oxyethylene)]/ $LiClO_4$ Polymer Electrolytes, *J. Electrochem. Soc.*, 1992, **139**, 3046.

73 C. Shen, Q. Zhao, N. Shan, B. B. Jing and C. M. Evans, Conductivity–Modulus– T g Relationships in Solvent-free, Single Lithium Ion Conducting Network Electrolytes, *J. Polym. Sci.*, 2020, **58**(17), 2376–2388, DOI: 10.1002/pol.20200302.

74 L. E. Porath and C. M. Evans, Importance of Broad Temperature Windows and Multiple Rheological Approaches for Probing Viscoelasticity and Entropic Elasticity in Vitrimers, *Macromolecules*, 2021, **54**(10), 4782–4791, DOI: 10.1021/acs.macromol.0c02800.

75 M. Capelot, M. M. Unterlass, F. Tournilhac and L. Leibler, Catalytic Control of the Vitrimer Glass Transition, *ACS Macro Lett.*, 2012, **1**(7), 789–792, DOI: 10.1021/mz300239f.

76 H. Zheng, Q. Liu, X. Lei, Y. Chen, B. Zhang and Q. Zhang, A Conjugation Polyimine Vitrimer: Fabrication and Performance, *J. Polym. Sci. A Polym. Chem.*, 2018, **56**(22), 2531–2538, DOI: 10.1002/pola.29232.

77 J. Liu, X. Liu, X. Cui, J. Qin, M. Shi, D. Wang, L. Liang and C. Yang, Imine-Containing Epoxy Vitrimer Cured by Active Ester: Properties and Theoretical Analysis, *ACS Appl. Polym. Mater.*, 2023, **5**(12), 10042–10052, DOI: 10.1021/acsapm.3c01917.

78 B. Soman and C. M. Evans, Effect of Precise Linker Length, Bond Density, and Broad Temperature Window on the Rheological Properties of Ethylene Vitrimers, *Soft Matter*, 2021, **17**(13), 3569–3577, DOI: 10.1039/d0sm01544j.

79 G. P. Carden, M. L. Martins, G. Toleutay, S. Cheng, B. Blad, J. Foster, C. Gainaru and A. P. Sokolov, Critical Role of the Steric Factor in the Viscoelasticity of Vitrimers, *Macromolecules*, 2025, **58**(11), 5494–5504, DOI: 10.1021/acs.macromol.5c00552.

80 J. Liu, J. J. Li, Z. H. Luo and Y. N. Zhou, Mapping Crosslinking Reaction–Structure–Property Relationship in Polyether-Based Vinylogous Urethane Vitrimers, *AIChE J.*, 2022, **68**(4), DOI: 10.1002/aic.17587.

81 C. D. Robitaille and D. Fauteux, Phase Diagrams and Conductivity Characterization of Some PEO-LiX Electrolytes, *J. Electrochem. Soc.*, 1986, **133**(2), 315–325, DOI: 10.1149/1.2108569.

82 J. Liu, J. J. Li, Z. H. Luo and Y. N. Zhou, Fast Room-temperature Self-healing Vitrimers Enabled by Accelerated Associative Exchange Kinetics, *Chem. Eng. J.*, 2023, **452**, 139452, DOI: 10.1016/j.cej.2022.139452.

83 J. R. Sangoro, C. Iacob, A. L. Agapov, Y. Wang, S. Berdzinski, H. Rexhausen, V. Strehmel, C. Friedrich, A. P. Sokolov and F. Kremer, Decoupling of Ionic Conductivity from Structural Dynamics in Polymerized Ionic Liquids, *Soft Matter*, 2014, **10**(20), 3536–3540, DOI: 10.1039/c3sm53202j.

84 K. Nakamura, K. Fukao and T. Inoue, Dielectric Relaxation and Viscoelastic Behavior of Polymerized Ionic Liquids with Various Counteranions, *Macromolecules*, 2012, **45**(9), 3850–3858, DOI: 10.1021/ma300040b.

85 Q. Zhao, C. Shen, K. P. Halloran and C. M. Evans, Effect of Network Architecture and Linker Polarity on Ion Aggregation and Conductivity in Precise Polymerized Ionic Liquids, *ACS Macro Lett.*, 2019, **8**(6), 658–663, DOI: 10.1021/acsmacrolett.9b00293.

86 S. Park, S. Yang and S. K. Kim, Dynamic Imine Bonds-Based Vitrimer Electrolytes for Stable Interfaces in Lithium Metal Electrodes, *ACS Appl. Polym. Mater.*, 2025, **7**(23), 16065–16072, DOI: 10.1021/acsapm.5c03253.

